

PAPER • OPEN ACCESS

Fast, high-fidelity readout of multiple qubits

To cite this article: N T Bronn *et al* 2017 *J. Phys.: Conf. Ser.* **834** 012003

View the [article online](#) for updates and enhancements.

Related content

- [High fidelity readout of a transmon qubit using a superconducting low-inductance undulator galvanometer microwave amplifier](#)
Yanbing Liu, Srikanth J Srinivasan, D Hover *et al.*
- [Quantum bits take the bus](#)
- [Measurement-induced entanglement of two superconducting qubits](#)
Jian Li, K Chalapati and G S Paraoanu

Recent citations

- [Rapid High-fidelity Multiplexed Readout of Superconducting Qubits](#)
Johannes Heinsoo *et al*



IOP | ebooks™

Bringing you innovative digital publishing with leading voices to create your essential collection of books in STEM research.

Start exploring the collection - download the first chapter of every title for free.

Fast, high-fidelity readout of multiple qubits

N T Bronn, B Abdo, K Inoue, S Lekuch, A D Córcoles, J B Hertzberg, M Takita, L S Bishop, J M Gambetta, J M Chow

IBM T.J. Watson Research Center, 1101 Kitchawan Rd, Yorktown Heights, NY, 10598, USA

E-mail: ntbronn@us.ibm.com

Abstract. Quantum computing requires a delicate balance between coupling quantum systems to external instruments for control and readout, while providing enough isolation from sources of decoherence. Circuit quantum electrodynamics has been a successful method for protecting superconducting qubits, while maintaining the ability to perform readout [1, 2]. Here, we discuss improvements to this method that allow for fast, high-fidelity readout. Specifically, the integration of a Purcell filter, which allows us to increase the resonator bandwidth for fast readout, the incorporation of a Josephson parametric converter, which enables us to perform high-fidelity readout by amplifying the readout signal while adding the minimum amount of noise required by quantum mechanics, and custom control electronics, which provide us with the capability of fast decision and control.

1. Introduction

Quantum computers have the potential to solve certain problems much more efficiently than classical computers [3, 4, 5]. In 1994, Peter Shor proposed a quantum algorithm to factor large composite numbers into their respective primes that is exponentially more efficient than any known classical algorithm [6]. This ignited additional interest into quantum computing, with more experimental effort into constructing the basic building blocks. The basic unit of information for a quantum computer is a quantum bit (qubit), which physically can be any two-level quantum mechanical system. The challenge is to control and measure qubits, while prohibiting unwanted interactions with their environment, and scaling them up to larger systems. Currently, the largest qubit systems are with trapped ions or superconducting circuits [7, 8, 9, 10].

2. Qubit Control

At IBM we use the *transmon* style of superconducting qubit, consisting of a single Al/AlO_x/Al Josephson junction shunted by a large capacitor [11]. The Josephson junction provides a nonlinear inductance which, when combined with the capacitive shunt, forms an anharmonic oscillator. In such a system, the lowest two energy levels can be used as the qubit and can be uniquely addressed as the |0⟩ and |1⟩ computational states. Qubit control is provided by applying microwave frequency pulses at this transition frequency, typically ∼4–6 GHz, which rotates the qubit state around the Bloch sphere about an axis that lies in the *xy*-plane (Fig. 1a). Applying a pulse that rotates the state by 180° would then take the |0⟩ state to the |1⟩ and vice versa. Thus, it is equivalent to the classical NOT gate in digital logic. If instead a 90° pulse is applied, the qubit state would be in an equal superposition of both |0⟩ and |1⟩. The phase of this superposition is set by the phase of the applied microwave-frequency tones. Because the



Content from this work may be used under the terms of the [Creative Commons Attribution 3.0 licence](#). Any further distribution of this work must maintain attribution to the author(s) and the title of the work, journal citation and DOI.

measurement of qubits projects the state into the z -axis, measuring this state would yield $|0\rangle$ in half of the cases and $|1\rangle$ in the other half.

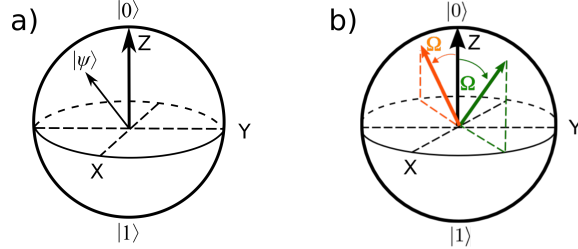


Figure 1. a) The qubit states $|0\rangle$ and $|1\rangle$ are represented on the Bloch sphere as the North and South poles, respectively. Any other point on the surface of the sphere represents a superposition of $|0\rangle$ and $|1\rangle$, with the equator being an equal superposition. b) Bloch sphere of the target qubit showing the dependence of its rotation direction on the state of the control qubit when the cross resonance operation is applied.

In order to complete a universal computational set of operations for quantum computing, there must also be operations between pairs of qubits. Such two-qubit gates can generate quantum entanglement between qubits, and the particular physical implementation we use is known as *cross-resonance gates* [12, 13, 14]. In a cross-resonance operation, a target qubit is driven via a control signal applied to a separate coupled qubit, known as the control qubit. When the two qubits are weakly coupled, such a microwave cross-resonance gate can result in a rotation of the target qubit that depends on the state of the control qubit (see Fig. 1b). Through proper adjustment of the target and control qubit microwave drive fields, it is possible to tune up a controlled-not (CNOT) entangling gate.

3. Qubit Readout

One particular architecture for realizing superconducting quantum processors is circuit quantum electrodynamics (QED), in which superconducting qubits are strongly coupled to microwave resonators [1, 2]. Circuit QED is a fantastic testbed for studying quantum optics and strong light-matter interactions, yet it also serves as a technique by which qubits can be controlled and read out effectively, while helping to isolate them from the outside environment. Superconducting qubits can be coupled to coplanar waveguide (CPW) resonators for readout and control, and also to one another, as shown in Fig. 2a. In the dispersive regime of qubit-resonator coupling the resonator frequency becomes qubit-state dependent, and thus through probing this resonator it becomes possible to discern the qubit state. Often we apply a readout tone at a frequency between the resonator frequencies corresponding to the $|0\rangle$ and $|1\rangle$ qubit states, and measure a state-dependent phase shift of the reflected readout tone. This type of measurement also has the advantage of leaving the qubit in the state it was measured, known as a *quantum non-demolition* (QND) measurement.

Figure 3 shows a standard readout chain used for the readout of superconducting qubits in a dilution refrigerator setup. Please note that the drawing does not show the attenuation and filtering configuration that is present on the input line for simplicity. In this scheme, the readout pulse propagates from left to right. It is first routed to a qubit/resonator system via a commercial three-port microwave circulator. The readout pulse interacts with the qubit/resonator system, reflects off the readout resonator, and carries information about the qubit state in its phase and amplitude. This readout signal is routed again, by the same three-port circulator, towards the output chain, where it passes through two wide-band isolators and a low-pass filter before it is amplified, first at the 3 K stage, by a high electron mobility transistor (HEMT) amplifier and

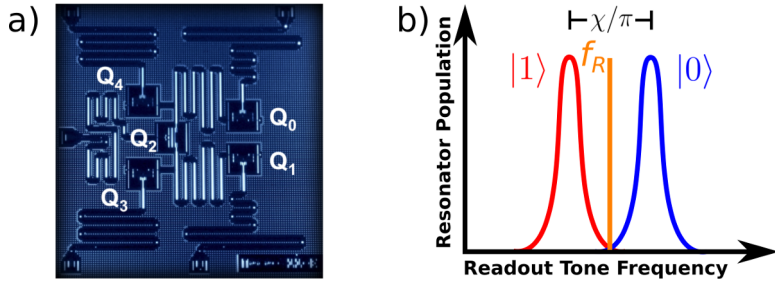


Figure 2. a) Micrograph of a five qubit processor, consisting of two bus resonators connecting the qubits and five readout resonators which are also used for control. b) Diagram of the qubit state dependence of the resonator, separated by the dispersive shift χ/π . The readout frequency f_R is typically set between the resonator's frequencies corresponding to the $|0\rangle$ and $|1\rangle$ states.

later at room temperature by commercial radio frequency (RF) amplifiers. Then, the amplified signal gets mixed down with a local oscillator (LO) to a low intermediate frequency (IF) on the order of tens of megahertz, digitized, and processed by a computer. We will repeatedly refer back to this readout chain in our discussion about improving it.

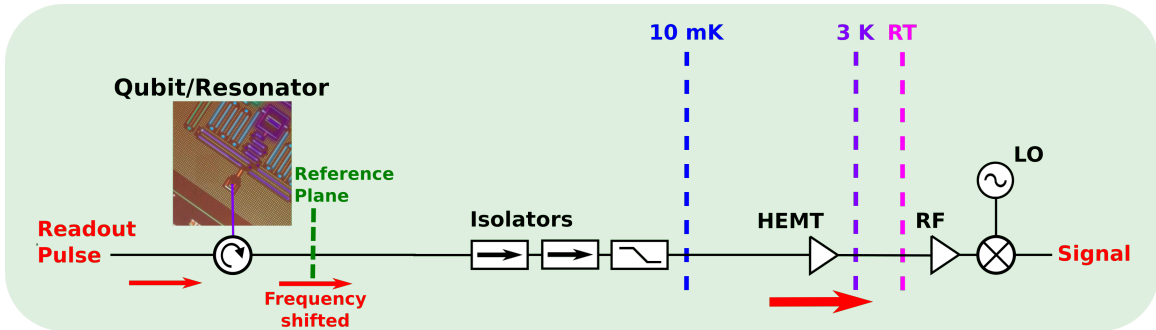


Figure 3. Standard readout scheme. A readout pulse is applied to the superconducting qubit/resonator system through an input line in the dilution refrigerator. The input line (not shown) includes several fixed attenuators and filters that are well-thermalized at different stages of the dilution refrigerator. The role of these attenuators and filters is to heavily attenuate the readout signal and noise coming from the room temperature instruments down to the level of a few microwave photons. This attenuated readout pulse is incident upon a microwave circulator that directs it to the qubit/resonator system, where it is reflected with a phase shift depending on the state-dependent resonance frequency of the resonator (we will refer signals back to the reference plane depicted here). The pulse then passes through two isolators and a low-pass filter, used to protect the device from noise coming down the output chain. The pulse is then amplified by a HEMT amplifier at the 3 K stage and further by room temperature RF amplifiers before it is mixed down with an LO to an IF and digitized.

4. Towards Fast, High-fidelity Readout

Fast, high-fidelity readout is crucial for building a quantum computer. While the standard scheme discussed thus far is sufficient to perform experiments in which measurements may be averaged over many rounds, carrying out more sophisticated experiments on a quantum computer which employ feedback and dynamic state-dependent operations is more challenging and require fast, high-fidelity readout [15, 16, 17]. For superconducting qubits, such a capability

can be realized by introducing three components: a Purcell filter that allows increased resonator bandwidth without adversely affecting the qubit lifetime, a Josephson parametric converter, which operates at the quantum limit (i.e., adds the minimum amount of noise required by quantum mechanics), for amplifying the readout tone, and logic and control electronics that facilitate quick measurement determination and feedback. The following sections describe each of these in further detail.

4.1. Purcell Filter

In standard circuit QED, one limitation on qubit lifetime, T_1 , is relaxation via spontaneous emission of a photon by the resonator, known as the Purcell effect. In this limitation, the qubit lifetime is inversely proportional to the qubit-resonator coupling strength and readout resonator bandwidth, κ . In particular, approximating the qubit as a harmonic oscillator, its spontaneous emission-limited lifetime is given by a generalized time constant $T_1^{\text{Purcell}} = C_q/\text{Re}[Y_q]$, where C_q is the capacitance of the qubit and Y_q is the admittance seen by the qubit at its transition frequency. In the case of standard QED, Y_q corresponds to the frequency-dependent admittance seen by the qubit, which depends on the readout resonator frequency and κ . To realize fast readout, κ should be large, so as to allow photons that carry information about the qubit state out of the system faster. Yet, increasing this parameter is at odds with the requirement of having a low rate of spontaneous emission, which enables longer qubit lifetimes. Fortunately, because the readout resonator frequency is detuned from the qubit transition frequency, a filter may be engineered that suppresses spontaneous emission (at the qubit transition frequency) while being transparent at the readout resonator frequency.

There are a number of ways of realizing this so-called Purcell filter, including the use of quarter-wave stubs [18], low- Q bandpass filters [19, 20], and the crosstalk between qubit and $50\ \Omega$ environment [21]. Our design takes the form of a stepped impedance Purcell filter (SIPF) consisting of alternating sections of low- and high-impedance (of Z_{lo} and Z_{hi} , respectively) CPW, shown in Fig. 4a [22]. The SIPF consists of five sections connected by $40\ \mu\text{m}$ tapers, with the low-impedance sections forming the ends. The measured (at 4.2 K) and modeled transmission and reflection characteristics of the SIPF drawn in Fig. 4b, show a passband around the readout resonator frequency at 6.4 GHz arising from the filter's resonant structure. Likewise, a large stopband from $\sim 2 - 6$ GHz, whose suppression increases with the number of sections in the SIPF and the impedance asymmetry $\alpha = Z_{hi}/Z_{lo}$, gives a suppression of 20 dB at a typical qubit frequency of 5 GHz. The fact that the SIPF may be placed on a separate die helps reduce spurious package modes [23] and opens the possibility of modular implementation.

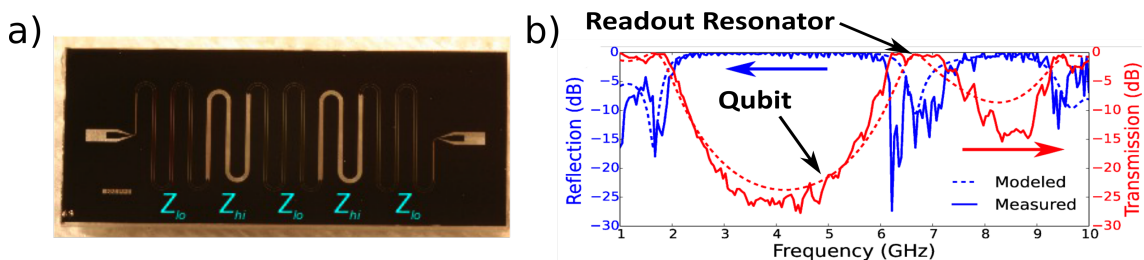


Figure 4. a) Five section SIPF consisting of alternating sections of CPW with impedance Z_{lo} and Z_{hi} . b) Modeled and measured transmission and reflection characteristics of the SIPF depict a passband around the readout resonator frequency and stopband around the qubit transition frequency. Adapted from Ref. [22].

We investigate the performance of the SIPF by studying a large- κ resonator coupled to a flux-tunable superconducting transmon device. The device and SIPF are backmounted to a printed

circuit board (PCB) by a copper push block, shown in Fig. 5. The PCB routes signals through internal $50\ \Omega$ buried stripline traces, which are wire-bonded at the openings of the windows to feedlines on the qubit/resonator device and SIPF. The length of the trace connecting the device and SIPF is tailored such that the lowest mode supported by the trace lies far below the qubit transition frequency. Qubit lifetime is modeled and measured and plotted in Fig. 5b. Here, the green line indicates the maximum lifetime without a Purcell filter. The blue dots are measured qubit lifetime showing an order of magnitude improvement over the green line, and agree well with a model including the Purcell filter and an intrinsic (i.e., not readout related) loss channel corresponding to a maximum lifetime of $T_1^{\text{intr}} \approx 55\ \mu\text{s}$ depicted in purple. This agrees with similar devices measured at IBM. The black curve corresponds to the maximum lifetime given only by the Purcell effect, indicating the potential for improving the qubit lifetime by another order of magnitude or two by addressing the intrinsic loss mechanisms of the qubit. Hence, the SIPF allows fast measurement without the concomitant degradation in qubit lifetime that comes from increased resonator linewidth. Further details can be found in Ref. [22].

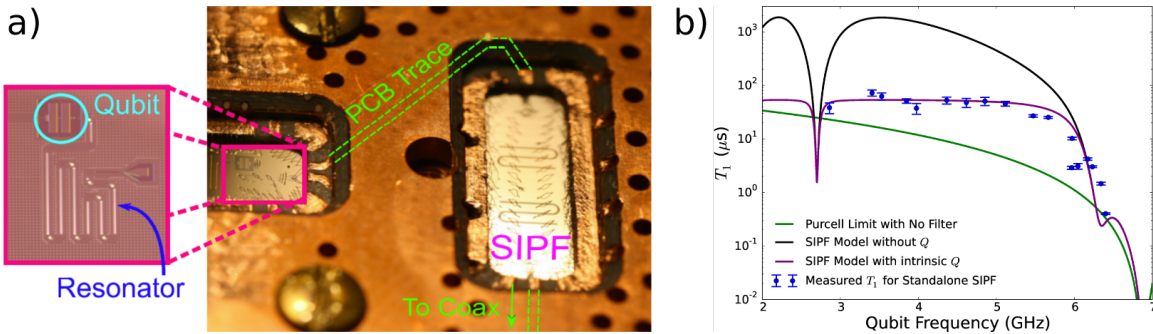


Figure 5. a) SIPF connected to a qubit device by a buried stripline $50\ \Omega$ PCB trace. b) Measured T_1 as a function of frequency of the device in a). Blue dots are measured data, which fits well with a T_1 model assuming an intrinsic $T_1^{\text{intr}} \approx 55\ \mu\text{s}$ in purple. The green (black) line corresponds to the T_1 limit of the device with (without) the SIPF. The mode around 3 GHz corresponds to the $50\ \Omega$ PCB trace. Adapted from Ref. [22].

4.2. Josephson Parametric Converter

The second component in our output scheme, which enables us to perform high-fidelity, single-shot measurement of the qubit state, is a Josephson parametric amplifier, known as the Josephson parametric converter (JPC) [24]. Before we explain how the integration of this preamplifier prior to the HEMT amplifier enables us to achieve this goal, it is important to briefly review the JPC physics and mode of operation. The JPC is a nondegenerate, three-wave mixing device capable of amplifying weak microwave signals at the quantum limit. It consists of two half-wave microwave transmission line resonators, as shown in the circuit diagram of the JPC in Fig. 6a and the JPC micrograph in Fig. 6b. The two resonators intersect in a Josephson ring modulator (JRM) at their centers. The JRM consists of four Josephson junctions arranged in a Wheatstone bridge configuration, which serves as a nonlinear, dispersive medium capable of performing three-wave mixing processes. The JRM has three eigenmodes: two differential and one common. The two differential modes are supported by the corresponding fundamental resonance mode of the JPC resonators, which we refer to as the signal and idler resonators. In order to operate the device as an amplifier, a strong, coherent microwave drive, referred to as the pump, is applied to the device whose frequency is the sum of the resonance frequencies of the signal and idler resonators. The pump drive gives rise to a common mode excitation of the JRM,

which leads to parametric amplification of the reflected signal and idler tones incident on the device ports. Since the JPC operates in reflection, a second circulator must be added between the circulator and isolators of Fig. 3 to route the signal to the JPC and then to the output line. In order to feed the signal, idler, and pump tones into the device, state-of-the-art JPCs employ two commercial, off-chip, broadband 180 degree hybrids as shown in Figs. 6a and 6c, which are connected to the feedlines of the signal and idler resonators. In this configuration, the signal and idler tones are fed through the Δ port of the corresponding hybrids, while the pump tone is fed through one of the Σ ports of the two hybrids (the Σ port of the other hybrid is terminated by 50Ω). Furthermore, in order for the JRM to operate as a three-wave mixing device, a dc circulating current in the outer loop of the JRM is needed to facilitate the interaction between the three modes. Such a circulating current can be induced by applying an external magnetic field through the JRM loop. In standard JPC devices, this magnetic flux is applied by using an external magnetic coil mounted on the JPC package, as shown in Fig. 6c. It is worthwhile noting that the main purpose of the four inner Josephson junctions of the JRM, shown in Fig. 6a, is to inductively shunt each Josephson junction of the JRM (that is on the external loop). The role of this inductive shunting is to lift the hysteretic response of the JRM versus flux and make the resonance frequencies of the JPC tunable [25].

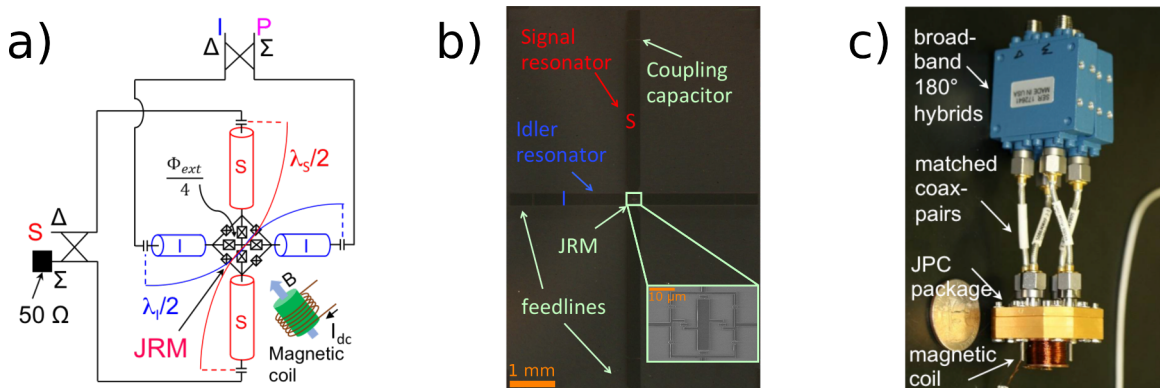


Figure 6. a) Standard JPC circuit. The JPC consists of two microwave resonators with different fundamental resonance modes, denoted signal (S) and idler (I). The two orthogonal resonators intersect in the middle at a JRM. The device circuit also includes two off-chip, broadband 180 degree hybrids and an external magnetic coil. b) Micrograph of a JPC device implemented using microstrip resonators, and c) A photo of a JPC device featuring the JPC package, the two hybrids, and the external magnetic coil.

Following this brief introduction of the JPC, we now turn to explain how the JPC allows us to achieve a high-fidelity, single-shot (i.e., without averaging over many rounds) readout of the qubit state. One simple way to explain it is using the illustration shown in Fig. 7, which qualitatively compares (not to scale) between the signal-to-noise ratio (SNR) of the output signal achieved using the “HEMT amplifier only” readout scheme versus the SNR achieved using the readout scheme which employs the “JPC as a preamplifier before the HEMT”. In the illustrations of Fig. 7, we represent the output microwave readout signals and the corresponding noise in the IQ -plane, where I and Q represent the two quadratures of the microwave field (which can be directly measured by mixing down the readout signal and integrating at room temperature). In Fig. 7a, we show an example of a readout signal at the reference plane that is dominated by vacuum noise and exhibits a symmetric superposition of $|0\rangle$ (blue, left) and $|1\rangle$ (red, right) states of the qubit. The blue and red circles represent 2D histograms of the qubit state measurements, which given a suitable binning, count the number of integrated shots that occur in each bin. In

this picture, the distance between the center of each 2D histogram (blue or red) and the origin (of the IQ -plane) represents the amplitude of the microwave signal, whereas the radius of the circle represents the standard deviation of the signal noise. In Fig. 7b, we show an illustration of the same readout signal as in Fig. 7a after being amplified by the HEMT and referred back to the reference plane. As can be seen in this figure, the added noise by the HEMT, which can be on the order of 20 input photons at the signal frequency, causes a very large overlap of the two 2D histograms representing the two qubit states, as the width of the 2D histograms are very large compared to the separation of the corresponding centers. As a result of this large overlap, the ability to distinguish with high-fidelity between the qubit states $|0\rangle$ and $|1\rangle$ is diminished. In contrast, by using a quantum-limited amplifier (QLA), such as the JPC, as a preamplifier before the HEMT, which adds noise on the order of a half input photon at the signal frequency, the SNR characterizing the readout signal, when referring back to the reference plane, is mainly dominated by the added noise of the preamplifier. This leads to a separation between the centers of the 2D histograms representing the qubit states, which exceeds their width. This, in turn, allows us to determine the qubit state with high fidelity using the integrated signal of a single measurement.

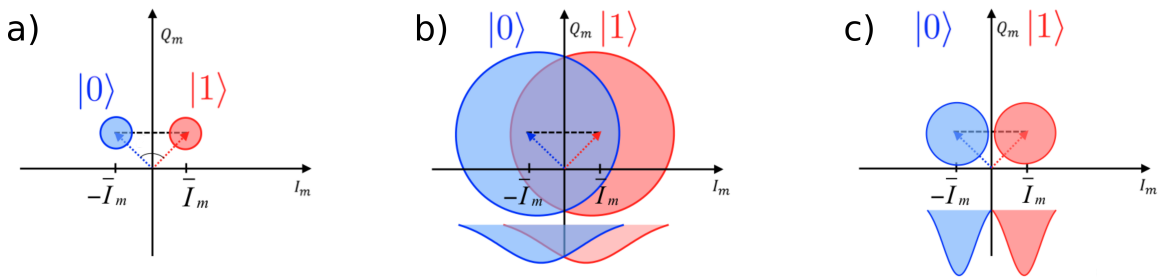


Figure 7. Illustrations that qualitatively show the 2D histograms of the signal and the corresponding noise in the IQ -plane for two different readout schemes as explained in the text (not to scale). In these illustrations, the readout signal carries information about the qubit state and the qubit is in an equal superposition of $|0\rangle$ and $|1\rangle$. a) A representation of the readout signal and the corresponding vacuum noise as seen at the reference plane (depicted in Fig. 3) before being amplified. b) A representation of the readout signal and corresponding noise in the “HEMT amplifier only” readout setup, when referred back to the reference plane. c) A representation of the readout signal and corresponding noise in the “JPC as a preamplifier before the HEMT” scheme, when referred back to the reference plane.

In Fig. 8, we demonstrate the ability to do fast, high-fidelity readout using a JPC amplifier and SIPF. The blue, red, and black curves of Fig. 8 represent double Gaussian fits to qubit-state histogram measurements, corresponding to the qubit being prepared in the $|0\rangle$, $|1\rangle$, and $|0\rangle + |1\rangle$ states, respectively. The readout measurements of the qubit are amplified by a JPC and HEMT. The achieved readout fidelity in this measurement is 96.5% with a measurement time $\tau_m = 370$ ns. Such a short measurement time is made possible due to the large readout resonator bandwidth (κ) of this device. Moreover, in this setup we retain a relatively long qubit lifetime (T_1) of 48 μ s, despite the large bandwidth of the readout resonator, that is due to the presence of the SIPF.

4.3. Logic and Control Electronics

The third component needed for running quantum algorithms with active feedback is fast decision and control. Current methods of using a digitizer connected to CPU over PCIe does not allow real-time processing of data, because of the data transfer overhead and incurred software

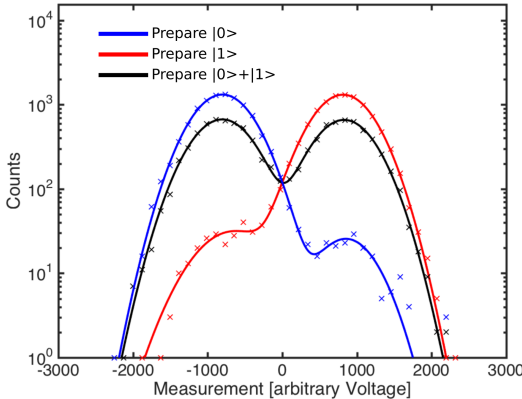


Figure 8. Readout histograms obtained by projecting 2D histogram measurements, as in Fig. 7, on the I -quadrature. The blue, red, and black curves represent double Gaussian fits to the histogram measurements of the qubit, after being prepared in the $|0\rangle$, $|1\rangle$, and $|0\rangle + |1\rangle$ states, respectively.

latency. Implementing logic directly on a Field Programmable Gate Array (FPGA), which has a deterministic latency because logic is performed in hardware within a fixed number of clock cycles, allows real time processing of data. Therefore, execution of decisions can be made based on measurement feedback with minimal latency. We implement logic on an FPGA connected to an analog-to-digital converter (ADC). The FPGA is also connected to a digital-to-analog converter (DAC) for stimulus for active control and a CPU over PCIe for testing. FPGA electronics for automated decision and control has recently become of interest to researchers in the quantum computing field because it enables low-latency signal processing in hardware [26, 27]. Our setup, consisting of modular components for testing and evaluation, is depicted in Fig. 9. Here, the IF signal is digitized and integrated using a matched filter [28], and thresholded to assign the value of $|0\rangle$ or $|1\rangle$ to the measurement. The histogram of this data is inset in Fig. 9 and indicates a readout fidelity of 95% when using both a JPC and HEMT for amplification and the SIPF. This is similar to readout fidelity using the standard digitizer. Current experiments involve active qubit reset, characterization of qubit stimulus from the DAC, and closing the loop to run the entire experiment from the FPGA. While current setups are done at room temperature, it is possible in the future that such decisions and control operations could be done at cryogenic temperatures [29].

5. Conclusion and Future of Readout Improvements

In summary, we presented three ingredients necessary to achieve fast, high-fidelity readout. A large resonator bandwidth for fast measurement without degrading the qubit lifetime is allowed by using an SIPF. Single-shot readout is facilitated by using a QLA, in our case a JPC in conjunction with a HEMT amplifier. And fast decision and control provided by a custom FPGA with ADC and DAC boards. Moreover, the FPGA can provide stimulus for active qubit reset and the large resonator bandwidth also aids in quickly clearing the cavity of readout photons.

As quantum processors become larger and contain more qubits, it becomes necessary to shrink and possibly eliminate as many microwave components as possible. For example, a new version of our JPC replaces the magnetic coil with an on-chip flux line, and uses an on-chip power divider to obviate the need for bulky hybrids [30]. Such a compact design is expected to be instrumental towards realizing directional amplifiers based on the JPC [24] and on-chip circulators [31, 32]. Current experiments at IBM involve one input and one output channel per

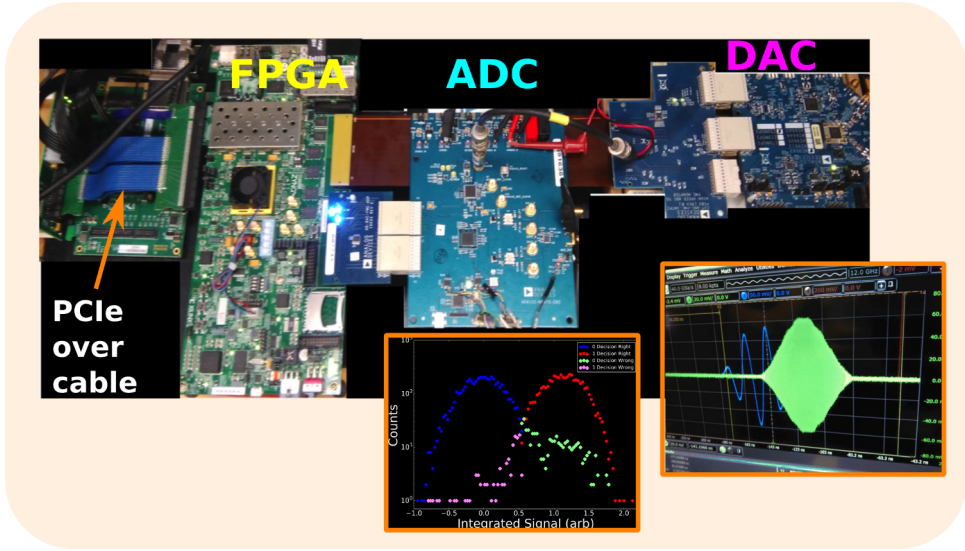


Figure 9. Custom control electronics. An FPGA is connected to a control computer (for testing) via a high-throughput PCIe over cable. Mounted on the FPGA is a ADC that integrates the readout signal using pre-calculated kernel weights of a matched filter and a DAC that can be used for stimulus, i.e. active qubit reset.

qubit, and schemes for adding more qubits per channel are being investigated. Furthermore, our group is exploring frequency multiplexing schemes, which would require the use of a wide-band QLA, such as a traveling wave parametric amplifier [33, 34], channel multiplexing, and fast microwave switching [35].

Acknowledgments

We thank M. Brink, M. B. Rothwell, and G. A. Keefe for fabrication of qubit devices and J. R. Rozen, J. Rohrs, and Y.-K.-K. Fung for experimental contributions. Work regarding the SIPF was done in conjunction with Y. Liu and A. A. Houck. We acknowledge support from IARPA under contract W911NF-10-1-0324.

References

- [1] Blais A, Huang R S, Wallraff A, Girvin S M and Schoelkopf R J 2004 *Physical Review A* **69** ISSN 1050-2947
- [2] Wallraff A, Schuster D I, Blais A, Frunzio L, Majer J, Kumar S, Girvin S M, Schoelkopf R J and Huang R S 2004 *Nature* **431** 162 ISSN 1476-4687
- [3] Shor P W 1997 *SIAM Journal on Computing* **26** 1484–1509 ISSN 0097-5397
- [4] Grover L K 1997 *Physical Review Letters* **79** 325 ISSN 0031-9007
- [5] Yung M H, Whitfield J D, Boixo S, Tempel D G and Aspuru-Guzik A 2014 Introduction to quantum algorithms for physics and chemistry *Advances in Chemical Physics* ed Kais S (Hoboken, New Jersey: John Wiley & Sons) pp 67–106
- [6] Shor P 1994 *Proceedings 35th Annual Symposium on Foundations of Computer Science* 124–134 ISSN 0272-5428
- [7] Chow J M, Gambetta J M, Corcoles A D, Merkel S T, Smolin J A, Rigetti C, Poletto S, Keefe G A, Rothwell M B, Rozen J, Ketchen M B and Steffen M 2012 *Physical Review Letters* **109** 060501 ISSN 0031-9007
- [8] Barends R, Kelly J, Megrant A, Veitia A, Sank D, Jeffrey E, White T C, Mutus J, Fowler A G, Campbell B, Chen Y, Chen Z, Chiaro B, Dunsworth A, Neill C, O’Malley P J J, Roushan P, Vainsencher A, Wenner J, Korotkov A N, Cleland A N and Martinis J M 2014 *Nature* **508** 500 ISSN 0028-0836
- [9] Harty T P, Allcock D T C, Ballance C J, Guidoni L, Janacek H A, Linke N M M, Stacey D N and Lucas D M 2014 *Physical Review Letters* **113** 2–6 ISSN 10797114
- [10] Nigg D, Müller M, Martinez E A, Schindler P, Hennrich M, Monz T, Martin-Delgado M A, Blatt R, Muller

M, Martinez E A, Schindler P, Hennrich M, Monz T, Martin-Delgado M A and Blatt R 2014 *Science* **345** 302–305 ISSN 1095-9203

- [11] Koch J, Yu T M, Gambetta J M, Houck A A, Schuster D I, Majer J, Blais A, Devoret M H, Girvin S M and Schoelkopf R J 2007 *Physical Review A* **76** 042319 ISSN 1050-2947
- [12] Paraoanu G S 2006 *Physical Review B* **74** 140504 ISSN 1098-0121
- [13] Rigetti C and Devoret M H 2010 *Physical Review B* **81** 134507 ISSN 1098-0121
- [14] Chow J M, Corcoles A D, Gambetta J M, Rigetti C, Johnson B R, Smolin J A, Rozen J R, Keefe G A, Rothwell M B, Ketchen M B and Steffen M 2011 *Physical Review Letters* **107** 080502 ISSN 0031-9007
- [15] Zhou X Q, Kalasuwani P, Ralph T C and O'Brien J L 2013 *Nature Photonics* **7** 223 ISSN 1749-4885
- [16] Elitzur A C and Vaidman L 1993 *Foundations of Physics* **23** 987–997 ISSN 0015-9018
- [17] Kwiat P, Weinfurter H, Herzog T, Zeilinger A and Kasevich M 1995 *Annals of the New York Academy of Sciences* **755** 383–393 ISSN 00778923
- [18] Reed M D, Johnson B R, Houck A A, DiCarlo L, Chow J M, Schuster D I, Frunzio L and Schoelkopf R J 2010 *Applied Physics Letters* **96** 203110 ISSN 00036951
- [19] Jeffrey E, Sank D, Mutus J Y, White T C, Kelly J, Barends R, Chen Y, Chen Z, Chiaro B, Dunsworth A, Megrant A, O'Malley P J J, Neill C, Roushan P, Vainsencher A, Wenner J, Cleland A N and Martinis J M 2014 *Physical Review Letters* **112** 190504 ISSN 0031-9007
- [20] Kelly J, Barends R, Fowler A G, Megrant A, Jeffrey E, White T C, Sank D, Mutus J Y, Campbell B, Chen Y, Chen Z, Chiaro B, Dunsworth A, Hoi I C, Neill C, O'Malley P J J, Quintana C, Roushan P, Vainsencher A, Wenner J, Cleland A N and Martinis J M 2015 *Nature* **519** 66 ISSN 0028-0836
- [21] Bronn N T, Magesan E, Masluk N A, Chow J M, Gambetta J M and Steffen M 2015 *IEEE Transactions on Applied Superconductivity* **25** 1700410 ISSN 1051-8223
- [22] Bronn N T, Liu Y, Hertzberg J B, Corcoles A D, Houck A A, Gambetta J M and Chow J M 2015 *Applied Physics Letters* **107** 172601 ISSN 0003-6951
- [23] Srinivasan S J, Corcoles A D, Magesan E, Bronn N T, Hertzberg J, Gambetta J M, Steffen M and Chow J M 2015 *Bulletin of the American Physical Society* **60** BAPS.2015.MAR.J39.4
- [24] Abdo B, Sliwa K, Frunzio L and Devoret M 2013 *Physical Review X* **3** 031001 ISSN 2160-3308
- [25] Roch N, Flurin E, Nguyen F, Morfin P, Campagne-Ibarcq P, Devoret M H and Huard B 2012 *Physical Review Letters* **108** 147701 ISSN 0031-9007
- [26] Ofek N, Petrenko A, Heeres R, Reinhold P, Leghtas Z, Vlastakis B, Liu Y, Frunzio L, Girvin S M, Jiang L, Mirrahimi M, Devoret M H and Schoelkopf R J 2016 *Nature* **536** 441 ISSN 0028-0836
- [27] Bultink C C, Rol M A, O'Brien T E, Fu X, Dikken B C S, Dickel C, Vermeulen R F L, de Sterke J C, Bruno A, Schouten R N and DiCarlo L 2016 *Physical Review Applied* **6** 034008 ISSN 2331-7019
- [28] Ryan C A, Johnson B R, Gambetta J M, Chow J M, da Silva M P, Dial O E and Ohki T A 2015 *Physical Review A* **91** 022118 ISSN 1050-2947
- [29] Colless J I and Reilly D J 2012 *Review of Scientific Instruments* **83** 023902 ISSN 00346748
- [30] Abdo B, Chavez-Garcia J M, Brink M, Keefe G and Chow J M 2016 (*Preprint arXiv:1609.00401*)
- [31] Kerckhoff J, Lalumière K, Chapman B J, Blais A and Lehnert K K 2015 *Physical Review Applied* **4** 034002 ISSN 2331-7019
- [32] Sliwa K M, Hatridge M, Narla A, Shankar S, Frunzio L, Schoelkopf R J and Devoret M H 2015 *Physical Review X* **5** 041020 ISSN 2160-3308
- [33] Macklin C, O'Brien K, Hover D, Schwartz M E, Bolkhovsky V, Zhang X, Oliver W D and Siddiqi I 2015 *Science* ISSN 0036-8075
- [34] Vissers M R, Erickson R P, Ku H S, Vale L, Wu X, Hilton G C and Pappas D P 2016 *Applied Physics Letters* **108** 012601 ISSN 0003-6951
- [35] Pechal M, Besse J C, Mondal M, Oppliger M, Gasparinetti S and Wallraff A 2016 (*Preprint arXiv:1606.01031*)